

www.advanced-bio.com

Expressing Optogenetic Actuators Fused to N-terminal Mucin Motifs Delivers Targets to Specific Subcellular **Compartments in Polarized Cells**

Jiali Wang, Eric Platz-Baudin, Erik Noetzel, Andreas Offenhäusser, and Vanessa Maybeck*

Optogenetics is a powerful approach in neuroscience research. However, other tissues of the body may benefit from controlled ion currents and neuroscience may benefit from more precise optogenetic expression. The present work constructs three subcellularly-targeted optogenetic actuators based on the channelrhodopsin ChR2-XXL, utilizing 5, 10, or 15 tandem repeats (TR) from mucin as N-terminal targeting motifs and evaluates expression in several polarized and non-polarized cell types. The modified channelrhodopsin maintains its electrophysiological properties, which can be used to produce continuous membrane depolarization, despite the expected size of the repeats. This work then shows that these actuators are subcellularly localized in polarized cells. In polarized epithelial cells, all three actuators localize to just the lateral membrane. The TR-tagged constructs also express subcellularly in cortical neurons, where TR5-ChR2XXL and TR10-ChR2XXL mainly target the somatodendrites. Moreover, the transfection efficiencies are shown to be dependent on cell type and tandem repeat length. Overall, this work verifies that the targeting motifs from epithelial cells can be used to localize optogenetic actuators in both epithelia and neurons, opening epithelia processes to optogenetic manipulation and providing new possibilities to target optogenetic tools.

J. Wang^[+], A. Offenhäusser, V. Maybeck Institute of Biological Information Processing IBI-3 Forschungszentrum Jülich GmbH 52428 Jülich, Germany E-mail: v.maybeck@fz-juelich.de

J. Wang^[+], A. Offenhäusser Faculty of Mathematics Computer Science and Natural Sciences **RWTH Aachen University** 52062 Aachen, Germany E. Platz-Baudin, E. Noetzel Institute of Biological Information Processing IBI-2 Forschungszentrum Jülich GmbH 52428 Jülich, Germany

The ORCID identification number(s) for the author(s) of this article can be found under https://doi.org/10.1002/adbi.202300428

[+] Present address: School of Basic Medical Sciences, Shanxi Medical University, Taiyuan 030001, China

 $\ \ \, \bigcirc$ 2023 The Authors. Advanced Biology published by Wiley-VCH GmbH. This is an open access article under the terms of the Creative Commons Attribution License, which permits use, distribution and reproduction in any medium, provided the original work is properly cited.

DOI: 10.1002/adbi.202300428

1. Introduction

In recent years, neuroscience has thrived by utilizing optogenetics, where optical and genetic methods combine to monitor (optogenetic sensor) or control (optogenetic actuator) cellular activity.[1] Optogenetics has also started to make inroads into cardiac research.[2] Optogenetics boasts high temporal and spatial precision in comparison to classical techniques such as pharmacological and extracellular electrical stimulation, respectively. Furthermore, optical control is less invasive than penetrating electrodes. However, wild types of optogenetic actuators are usually distributed throughout the cells. In general, this reduces the cells of interest for optogenetic channels. Polarized cells have vital morphological and functional compartmentalization. For epithelia, controlling ion currents specifically on either the apical or basolateral membrane would be a new application of optogenetic channels, further expanding their usefulness.

Cells utilize various methods to distribute membrane proteins to subcellular membrane regions, establishing and maintaining morphological and functional properties. For example, epithelial cells differentiate the basolateral and apical membranes, likewise, neurons differentiate and maintain the somatodendritic and axonal membranes. Compartmentalization is achieved by polarized trafficking, stabilization at desired locations, degradation at undesired locations, or collection of new proteins from one domain and transport to another domain.[2] During polarized trafficking, specific peptide sequences selectively sort proteins in the trans-Golgi network.[3] Some sorting principles are conserved between epithelia and neurons. So far, most of the published subcellular plasma membrane-targeted optogenetic actuators have focused on utilizing targeting motifs identified in neurons, such as the motifs from myosin binding domain, [4,5] II-III loop of the sodium channel^[6,7] and voltage-gated potassium channel.[8] Wide uptake of these constructs is hindered by their typically lower currents or incomplete targeting. However, sorting motifs from epithelial cells are also potentially useful considering the conserved targeting mechanisms between tissues. Examples of basolateral signals that are also somatodendritic, as well as apical sorting signals that are also axonal, can be found in **ADVANCED** SCIENCE NEWS

www.advancedsciencenews.com

ADVANCED BIOLOGY

www.advanced-bio.com

the literature.^[9–14] This could expand the use of optogenetics in additional cell types, as well as provide additional motifs to promote engineering other constructs.

To test epithelial motif targeting of optogenetic actuators in multiple cell types, we combine tandem repeats (TR) from Human mucin1 (MUC1) with the high current optogenetic channel Channelrhodopsin-2 XXL (ChR2-XXL, channel plus yellow fluorescent protein (YFP) tag). MUC1 is a sialylated transmembrane glycoprotein in glandular epithelial cells, whose large, highly glycosylated extracellular domain forms a rod-like structure. A prominent feature of the MUC1 ectodomain is the variable number of 20 amino acid long TRs: GSTAPPAHGVTSAPDTRPAP.[15] Core-glycosylated, mucin-like repeats have been reported as apical targeting signals, localizing MUC1 to the apical side of epithelial cells.[16,17] Therefore, we tested if TRs can localize optogenetic actuators without negative effects on achievable current. For the optogenetic actuator, we use a variant of Channelrhodopsin-2 (ChR2).[18,19] In ChR2, the residue Asp156 in helix 4 forms a hydrogen bond with Cys128 in helix 3, known as the DC gate, involved in channel closing.[20-23] The mutation in these two residues alters the kinetics of ChR2 channeling. The variant ChR2-XXL (D156C) has higher expression and a long open-state lifetime, currently providing the highest photostimulation efficiency while still spontaneously closing.^[24] It is suitable for the prolonged induction of depolarization without continuous illumination.[25,26]

Currently, most known modifications of channelrhodopsins for subcellular localization rely on replacing the C-terminus^[4–8] owing to the existing knowledge that there is conduction of irrelevant globular C-terminal domain in the naturally occurring protein.[19] However, the N-terminal targeting motifs may likewise be worth paying attention to if N-terminal tagged channels are shown to have consistent current properties. Here, we fused N-terminal targeting motifs 5 TR, 10 TR, and 15 TR from MUC1 to ChR2-XXL, producing three new actuators: TR5-ChR2XXL, TR10-ChR2XXL, and TR15-ChR2XXL, respectively. We demonstrate the currents and channel dynamics of the constructs using whole cell patch clamp recordings with defined membrane area of illumination in unpolarized and polarized kidney cell lines (Human Embryonic Kidney (HEK293) and Madin-Darby Canine Kidney (MDCK II), respectively). Furthermore, the unspecific localization in unpolarized HEK293, versus the lateral localization in polarized MDCK II is shown. Consistency of localization behavior was further shown for an additional nonpolarized cell (the cardiomyocyte-like HL-1) and MCF 10A cells polarized in spheroids. Somato-dendritic localization in neurons is shown and the transfection efficiencies (TEs) in kidney cells and neurons across different TR lengths were compared. Overall, we show that N-terminal motifs do not significantly interfere with channel function yet control localization in multiple cell types, providing new perspectives for subcellular research in polarized cells.

2. Results

2.1. Construct Generation

In this work, different numbers of tandem repeats (TR5, TR10, and TR15) from the extracellular region of MUC1 were chosen as

targeting motifs. Mucin genes are hard to synthesize artificially, due to the repetition, especially for TR15. Codon optimization was performed with manual adjustments to code synthesizable DNA. Then TRs were attached to the N-terminus of ChR2-XXL using seamless cloning. Cytomegalovirus (CMV) promoter, was used for strong, constitutive expression in mammalian cells. YFP at the C-terminal of ChR2-XXL was used for the localization of the constructs. Furthermore, the plasmids with TRs were hard to produce in Escherichia coli. After testing several strains, NEB Stable Competent *E.coli* proved suitable for the isolation of plasmid clones containing repeat elements. Finally, we obtained three new plasmids encoding TR5-ChR2XXL-YFP, TR10-ChR2XXL-YFP and TR15-ChR2XXL-YFP (hereafter TR5-ChR2XXL, TR10-ChR2XXL and TR15-ChR2XXL, respectively) (Figure 1A). The results were confirmed by DNA sequencing and restriction enzyme digestion.

2.2. Electrophysiological Characterization

One concern regarding N-terminal tagging of ChR2 variants is stearic hindrance of conduction by the tag. To evaluate if the TR-tagged optogenetic actuators have altered conduction, they were introduced into Human Embryonic Kidney 293 (HEK293) cells for whole-cell patch clamp measurements. This cell line is a useful system for electrophysiology studies due to its low expression of native channels. Since the HEK293 are not polarized cells, a fixed illumination area could consistently probe comparable areas of channel expression in the membrane. Whole-cell patch clamp was subsequently carried out on MDCK II cells to evaluate if the subcellular redistribution of channels alters whole-cell currents achieved per area of membrane illuminated.

2.2.1. Current-Voltage Relationship of the Membrane

We first test if overexpression causes changes in intrinsic cell membrane properties due to membrane composition or cell stress. The membrane's current-voltage relationship was measured via a whole-cell patch clamp in the dark (channels closed) for HEK293 cells expressing each construct. Figure 1B shows a typical voltage trace triggered by current injection from -200 pA to 400 pA at 50 pA intervals in HEK293 cells expressing ChR2-XXL. The voltage traces obtained in other groups expressing TR-ChR2XXL were all similar to this (data not shown). The currentvoltage relationship plots steady-state membrane voltage amplitudes versus injected currents, as shown in Figure 1C. Though at high current injections, the average membrane resistance in untagged ChR2-XXL is slightly lower than TR-ChR2XXLs in Figure 1C, this difference is not statistically significant. This suggests that TR-ChR2XXL expression in the closed state does not alter the cell membrane of HEK293 cells and currents can be attributed to channel function when opened.

2.2.2. Record in Different Clamp Modes

For optogenetic manipulation, we illuminated the expressing HEK293 cells with 1000 ms laser pulses for 20 overlays, separated by 1000 ms dark intervals, and recorded in voltage-clamp

27010198, 2024, 3, Downloaded

from https://onlinelibrary.wiley.com/doi/10.1002/adbi.202300428 by Forschungszentrum Jülich GmbH Research Center, Wiley Online Library on [25.03/2024]. See the Terms and Conditions (https://onlinelibrary.wiley.com/doi/10.1002/adbi.202300428 by Forschungszentrum Jülich GmbH Research Center, Wiley Online Library on [25.03/2024]. See the Terms and Conditions (https://onlinelibrary.wiley.com/doi/10.1002/adbi.202300428 by Forschungszentrum Jülich GmbH Research Center, Wiley Online Library on [25.03/2024]. See the Terms and Conditions (https://onlinelibrary.wiley.com/doi/10.1002/adbi.202300428 by Forschungszentrum Jülich GmbH Research Center, Wiley Online Library on [25.03/2024]. See the Terms and Conditions (https://onlinelibrary.wiley.com/doi/10.1002/adbi.202300428 by Forschungszentrum Jülich GmbH Research Center, Wiley Online Library.

onditions) on Wiley Online Library for rules of use; OA articles are governed by the applicable Creative Commons License

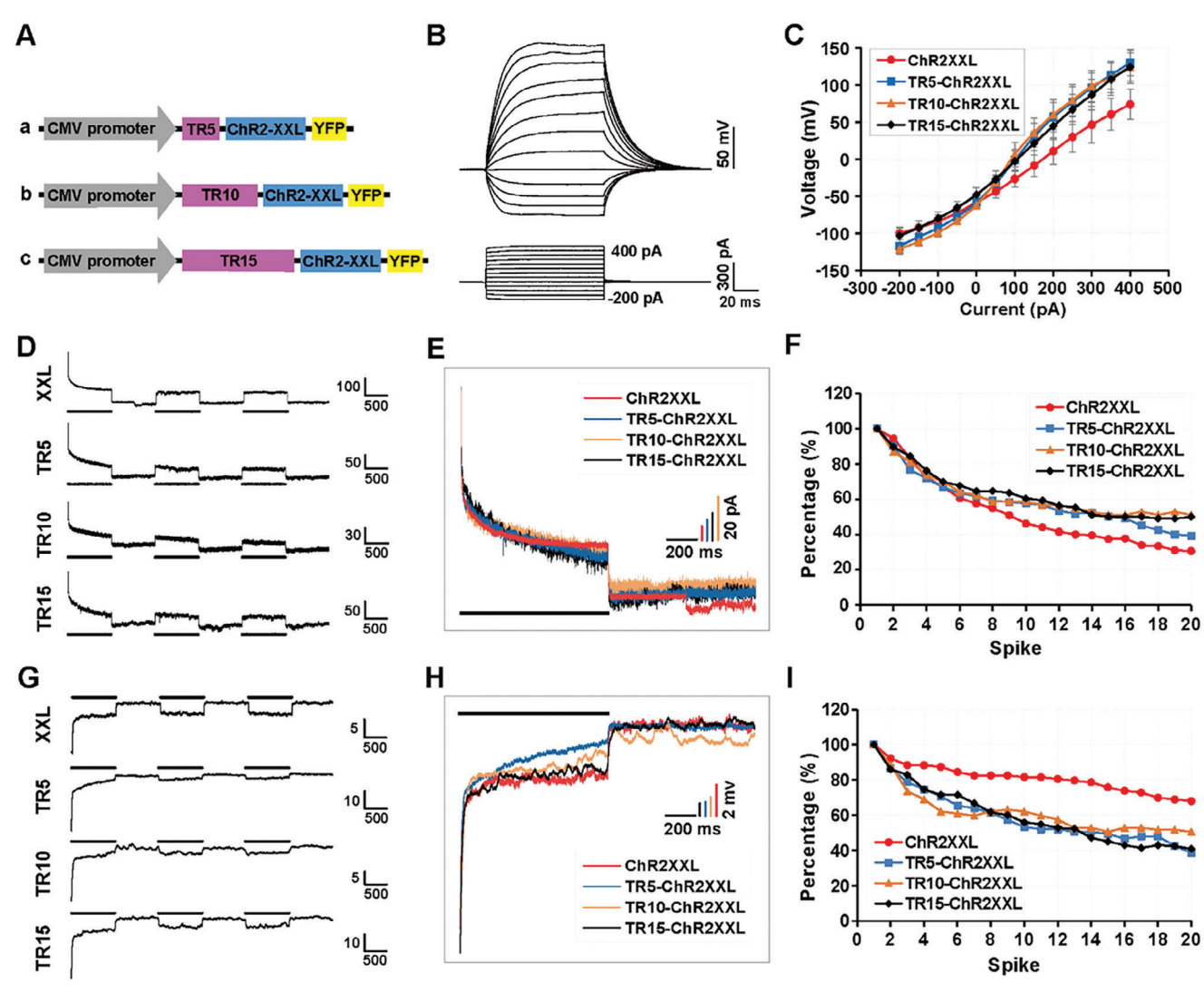


Figure 1. Actuator constructs and the electrophysiological characterization in cells. A) Schematic actuator constructs with CMV promoter, a) TR5, b)TR10, and c) TR15 from human mucin, a KLAT linker between TR and ChR2-XXL, and PAAAT linker between ChR2-XXL and YFP. B) A typical voltage profile in HEK293 cells expressing ChR2-XXL in response to current injection from -200 pA to 400 pA in 50 pA steps for 100 ms in the dark. C) Current-voltage relationship (mean \pm SEM) for HEK293 expressing different actuators. N=8, 9, 11, and 8 for ChR2-XXL, TR5-ChR2XXL, TR10-ChR2XXL, and TR15-ChR2XXL, respectively. Two-way repeated ANOVA test, p=0.472>0.05. D) HEK293 current traces (scale pA per ms) in v-clamp mode during 1 s on and 1 s off illumination. $V_{\text{hold}}=-60$ mV. E) Magnified current trace from the first light pulse in (D). F) The ratio of the current change elicited by the 2nd to 20th light pulses versus the first small additional peak. G) HEK293 voltage traces (scale mV per ms) in c-clamp mode during 1 s on and 1 s off illumination. $I_{\text{hold}}=-60$ pA. H) Magnified voltage trace from the first light pulse in (G). I) The ratio of the voltage change elicited by the 2nd to 20th light pulses versus the first small additional peak. In certain figures, ChR2-XXL, TR5-ChR2XXL, TR10-ChR2XXL, and TR15-ChR2XXL are shortened as XXL, TR5, TR10, and TR15, respectively, which applies to all figures in this article.

mode. The first three sequential activations of the channel in typical traces are displayed in Figure 1D and the zoom-in picture of the first spikes is shown in Figure 1E. Once illuminated, the currents increased rapidly at first, then gradually plateaued. At light-off, a small current increase appeared. Then the channels closed extremely slowly. After a short dark period of 1 s, in response to the second light pulse, the currents returned to the original plateau level, leading to decreased current magnitude. The current traces of different actuators showed similar configurations, indicating that the electrophysiological characteristics of ChR2-XXL were not affected by TRs. The current changes elicited by the second to twentieth light pulses were quantitatively compared

with the first additional small current peak produced at light-off. Figure 1F shows that the current changes triggered by the laser light pulses decreased gradually with more stimulations. This indicates a slight loss of effectivity during this stimulation protocol over time as the proportion of channels in each photostate shifts (see Discussion 3.1).

The stimulation was repeated with recordings in currentclamp mode. Figure 1G shows the voltage traces during the first 3 channel activations, the first of which are zoomed in and shown together for comparison in Figure 1H. The voltages increased rapidly in response to the light, then became steady in continuous illumination. When the laser was switched off,

Figure 2. Kinetics of actuators in HEK293 cells. Current traces (scale pA per ms) from transfected HEK293 during 50 ms light pulses, separated by intervals of 1950 ms (A) or 3950 ms (D). $V_{hold} = -60$ mV. The magnified current traces triggered by the first (B) and second (C) light pulse at 1950 ms inter-pulse interval. E) The ratios of the current changes elicited by light pulses other than the first one to the first small additional peak in (A) or (D). Individual current amplitudes were normalized to the first small additional peak. F) The average ratios of subsequent current changes to the first small additional peak in (A) or (D). Data are mean \pm SD, n=19 for 1950 ms inter-pulse intervals and n=9 for 3950 ms inter-pulse intervals. Kruskal-Wallis ANOVA test, 1950 ms, p = 0.097 > 0.05; 3950 ms, p = 0.379 > 0.05. G) Inward currents in voltage-clamped HEK cells evoked by 10 s of blue light. H) Mean photocurrents in response to 10 s blue light, normalized to the ChR2-XXL current. N = 8, 12, 11 and 8. Data are mean ± SEM. Kruskal-Wallis ANOVA test, p=0.504>0.05. I) Average time constants of channel opening (τ_{on}) . Data are mean \pm SEM. N=11, 14, 17 and 11. $R^2>0.81$. One-way ANOVA test, p = 0.411 > 0.05. J) Average time constants of channel closing (τ_{off}). Data are mean \pm SEM. N = 7, 10, 14 and 7. $R^2 > 0.90$. One-way ANOVA test, p = 0.253 > 0.05.

XXL

TR5 TR10 TR15

the voltages rose quickly, then diminished gradually. The laser pulses after 1 s dark quenched the voltages to a level similar to the previously observed change in current. All actuators displayed similar voltage changes during this stimulation sequence. The voltage changes during the second to twentieth light pulses were normalized to the first small additional voltage peak as percentages, seen in Figure 1I. These data demonstrate that the TR motifs do not affect the achieved current per area membrane, cell depolarization, or accumulation of inactive channels of ChR2-XXL. We, therefore, conclude that TR-ChR2XXLs can induce the same amplitude of membrane changes as ChR2-XXL.

40

20

2.2.3. Properties of the Induced Photocurrent

Further recordings were made at different optogenetic stimulation intervals to determine the kinetics of the new constructs. Current traces were recorded in HEK293 cells illuminated with 50 ms light pulses and inter-pulse intervals of either 1950 or 3950 ms, leading to 0.5 Hz or 0.25 Hz stimulation frequencies, respectively. Figure 2A,D shows the respective current profiles elicited. The first and second spike traces recorded under 0.5 Hz stimulation (Figure 2A) are magnified in Figure 2B,C, respectively, as merged images of the four channelrhodopsins. As the plots show, all four channelrhodopsins show uniform current

10

XXL

TR5 TR10 TR15



ADVANCED BIOLOGY

www.advanced-bio.com

pulse shapes. For the 0.5 Hz stimulations, the current changes of channelrhodopsin evoked at the beginning of individual lighton (except the first one) were normalized to the small current peak at first light-off, and the normalized percentages were plotted in Figure 2E (lines with circles). The average percentages for each channel are shown in Figure 2F (left bars), which were all $\approx\!85\%$ of the first additional small spikes. For the 0.25 Hz stimulations, the corresponding results are shown in Figure 2E (lines with triangles) and Figure 2F (right bars) as well. The average values were $\approx\!65\%$, a little lower than that at 0.5 Hz stimulation. After staying in dark for 3950 ms, the state of channelrhodopsins was closer to the plateau state when blue light was on, leading to the smaller current changes compared to the 1950 ms inter-pulse intervals

The photocurrent is a critical factor determining the effectiveness of ChR2 membrane depolarization. Hence, the currents of these channels evoked by blue light were compared. In order to give channels enough time to open and close (Figures S1 and S2, Supporting Information), the pulse and wait time here were 10 s and 80 s, respectively. Figure 2G shows inward photocurrents of four actuators triggered by 10 s of light in HEK293 cells recorded in voltage-clamp mode. The histogram in Figure 2H presents the mean photocurrents generated by individual optogenetic tools, normalized to the ChR2-XXL group's current. Photocurrents in TR groups were all slightly smaller than the ChR2-XXL group, but there was no significant difference between groups.

The dynamics of current onset and offset often determine which channelrhodopsin variant is desired. For TRs to be a general tag system, they must not alter channel kinetics. The rate of channel opening upon illumination was denoted as on kinetics (τ_{on}) and the rate of channel closure after light offset was denoted as off kinetics (τ_{off}), both of which were determined by the exponential fit of the corresponding rising or decaying photo current traces. The $\tau_{\rm on}$ of TR5-ChR2XXL, TR10-ChR2XXL, and TR15-ChR2XXL were 3.57 \pm 0.25 ms, 3.94 \pm 0.26 ms and 3.88 \pm 0.34 ms, respectively, all slightly longer than ChR2-XXL (3.32 \pm 0.32 ms) (Figure 21). With more TR, the channel opened a little more slowly. However, there was no significant difference between these groups. For $au_{ ext{off}}$, the values of TR5-ChR2XXL, TR10-ChR2XXL, and TR15-ChR2XXL were 34.07 \pm 3.25 s, 37.81 \pm 2.50 s and 42.05 \pm 2.42 s, respectively (Figure 2]). The $\tau_{\rm off}$ of ChR2-XXL was 41.16 ± 2.95 s, which was comparable to other groups. There was no significant difference between these groups. Taken together, the various numbers of TRs do not have a remarkable impact on relevant kinetic parameters for the current generation.

2.2.4. Photocurrents in Polarized Cells

Polarized MDCK cells are widely used as models for studying epithelial polarity, trafficking, and tight junctions. Their advantages include the rapid growth rate, clear cell polarity, and suitability for use in advanced microscopic techniques. [29,30] MDCK cells were cultured on track etch membranes, resulting in much better differentiated and polarized monolayers (10–15 μ m tall) than those grown on solid plastic or glass substrates (3–5 μ m tall). [31] Cultures were chemically transfected with each of the constructs within two days of high-density plating and grew for ≈ 5 days to form a tight monolayer.

Patch clamp recordings in whole-cell configuration voltage clamp at -60 mV detected light-induced currents in the cell illuminated with a small spot of laser light. For a subcellularly targeted expression, one area of the membrane the size of the laser spot should produce current. For homogeneously expressed channels, activation is expected on both sides of the cell as light passes through (roughly double the area of membrane with channels is illuminated). The produced pico amps per µm² of illuminated membrane for TR5-ChR2XXL, TR10-ChR2XXL and TR15-ChR2XXL were 6.62 ± 2.59 , 7.59 ± 1.99 and 4.97 ± 1.28 pA μ m⁻², respectively; higher than the current in the ChR2-XXL group $(3.15 \pm 2.60 \text{ pA} \mu\text{m}^{-2})$, although there was no significant difference between these groups. If cells produce equal amounts of protein but TR-ChR2XXL is concentrated in the lateral membrane, one spot of illumination may reach more channels. Furthermore, the TR-ChR2XXL currents produced in MDCK cells were generally larger than that in HEK293 cells, which were accordingly 0.95 ± 0.12 , 0.83 ± 0.17 and 0.64 ± 0.12 pA μm^{-2} . In each cell group, the currents were all normalized to the current produced in ChR2-XXL group, as shown in Figure 3. The normalized currents of TR5-ChR2XXL or TR10-ChR2XXL in MDCK cells significantly differed from that of TR15-ChR2XXL in HEK cells, likely due to differences in protein density in the illuminated space. We attribute differences in MDCK current among the constructs to the number of channels expressed in the illuminated area rather than a lack of opening channels because channel dynamics were shown to be consistent across constructs. Channels per area are a compound effect of channel production and localization.

2.2.5. Electrophysiology Summary

The electrophysiology results show that the TR tag on the N-terminal of the ChR2-XXL does not significantly alter channel dynamics. In non-polarized cells, there was no significant change in current per area illuminated, while in polarized cells, TR5-ChR2XXL and TR10-ChR2XXL showed slight increases in current per area illuminated. TR15-ChR2XXL was significantly less than TR5-ChR2XXL or TR10-ChR2XXL, but still higher than untagged channel. Therefore, despite their size, and situation at the N-terminal, TR domains from MUC1 are suitable tags for channelrhodopsin proteins.

2.3. Subcellular Localization in Polarized Cells

2.3.1. Subcellular Localization in MDCK Cells

MDCK II cells, grown and transfected as described previously were subsequently immunostained (Figure 4) with Alexa Fluor 633 secondary antibody and primary antibody for podxl (gp135), an established apical membrane marker for MDCK cells. [32,33] DAPI stained the nuclei, indicating which side of the apical surface was intracellular, and therefore remaining membrane is basolateral. In each image, the top view and reconstructed orthogonal slices show the localization of TR-ChR2XXL relative to the apical membrane. The orientations of image layers in z-stacks are all the same, and the top and bottom layers are marked as T

27010198, 2024, 3, Downloaded

from https://onlinelibrary.wiley.com/doi/10.1002/adbi.202300428 by Forschungszentrum Jülich GmbH Research Center, Wiley Online Library on [25.03/2024]. See the Terms

iditions) on Wiley Online Library for rules of use; OA articles are governed by the applicable Creative Commons License

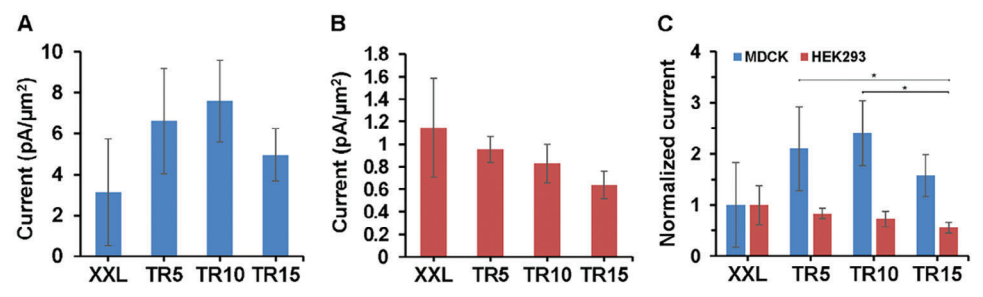


Figure 3. The currents produced in polarized and unpolarized cells. A) The currents of ChR2-XXL and TR-ChR2XXL elicited by 50 ms laser in MDCK cells. B) The currents of ChR2-XXL and TR-ChR2XXL evoked by 50 ms laser in HEK293 cells. C) The comparison of currents produced in MDCK and HEK293 cells. In each cell group, the currents were all normalized to the current of the ChR2-XXL. Data are presented as mean \pm SEM. Kruskal-Wallis ANOVA test, TR5-ChR2XXL (MDCK) versus TR15-ChR2XXL (HEK), *p = 0.014 < 0.05

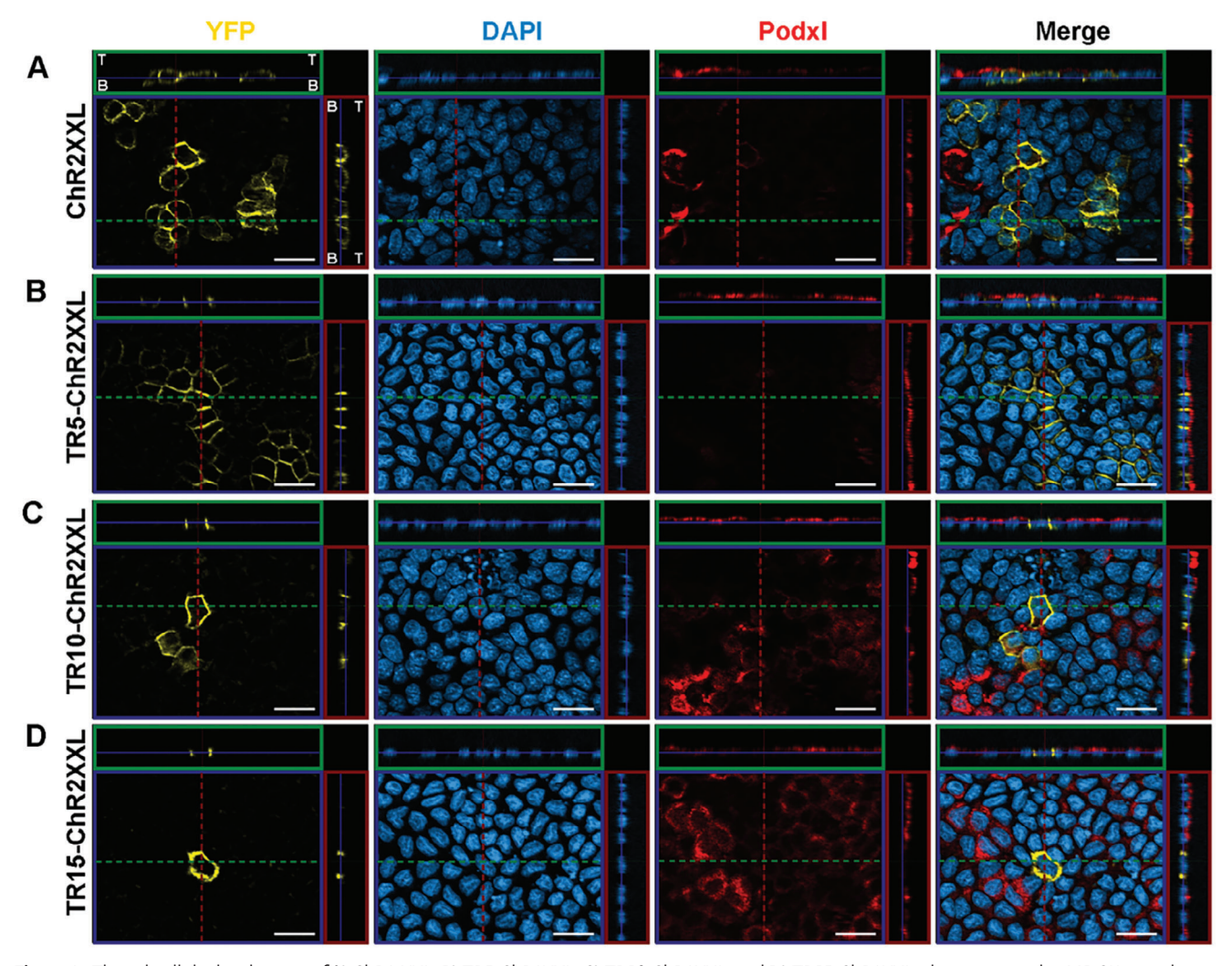


Figure 4. The subcellular localization of A) ChR2-XXL, B) TR5-ChR2XXL, C) TR10-ChR2XXL, and D) TR15-ChR2XXL when expressed in MDCK monolayers. Expressed channelrhodopsins were visualized by YFP (yellow). Cell nuclei were identified by DAPI staining (blue). The apical surface of MDCK cells was identified by antibody 3F2/D8 against Podxl (red). Merged images are shown in the last column. In each image, the top view of MDCK cells (at the focus level indicated by the blue line in small windows) is shown in the main window (xy plane), and vertical views of MDCK cells cut at green and red dashed lines are presented in the small green (xz plane) and red windows (yz plane). T, top – where apical surface touches medium; B, bottom – where cells adhere to the support membrane. Scale bar, 20 μm.

27010198, 2024, 3, Downloaded from https://onlinelibrary.wiley.com/doi/10.1002/adbi.202300428 by Forschungszentrum Jülich GmbH Research Center, Wiley Online Library on [25/03/2024]. See the Terms

on Wiley Online Library for rules of use; OA articles are governed by the applicable Creative Commons License

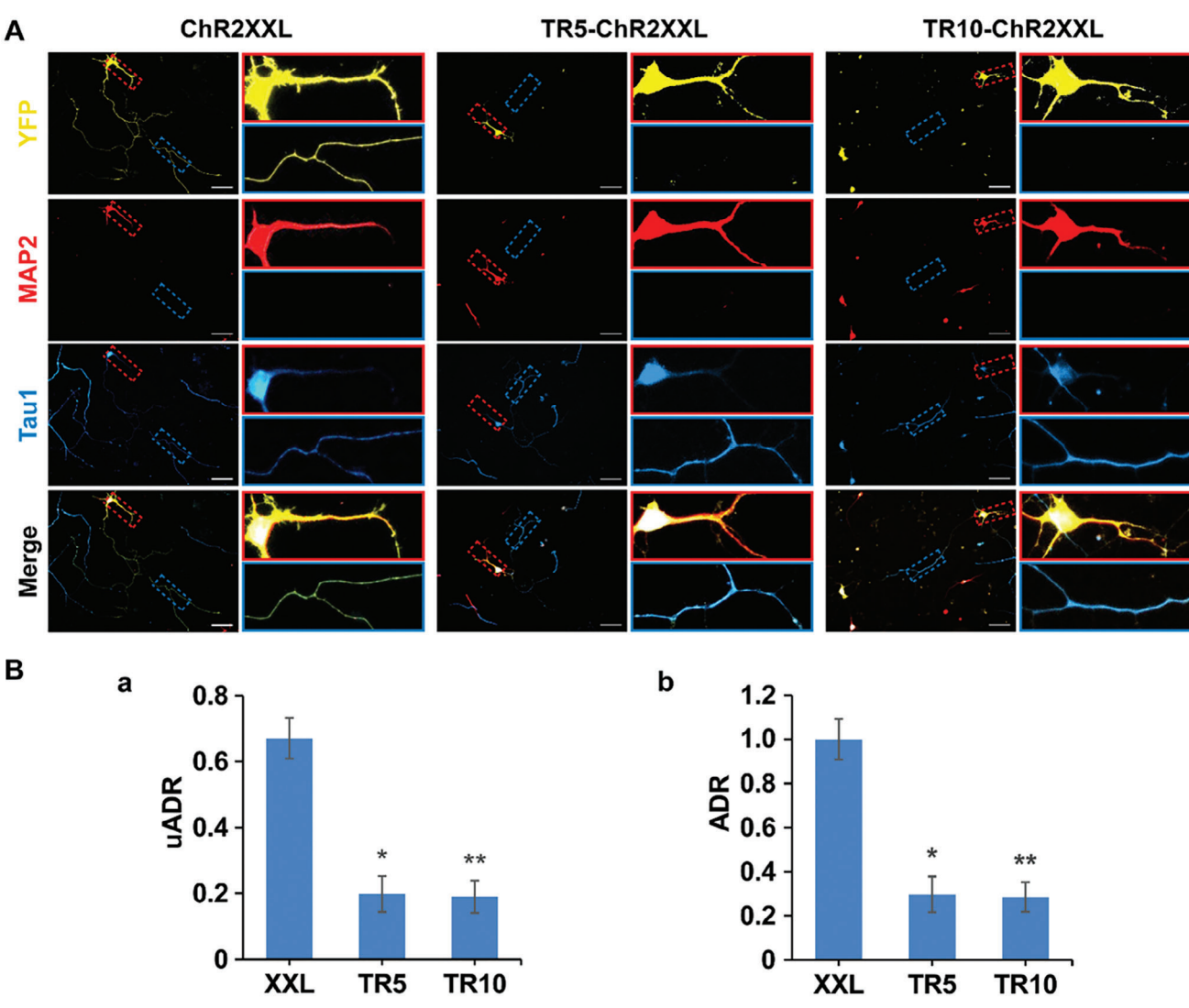


Figure 5. The subcellular localization of ChR2-XXL, TR5-ChR2XXL, and TR10-ChR2XXL when expressed in neurons. A) Immunostaining of transfected E18 cortical neurons (DIV5-7). Dendrites were labeled with anti-MAP2 (red) and axons with anti-Tau1 (blue). The red dashed box extracts a zoom of the somatodendritic region, rotated and displayed to the right. The blue dashed box extracts a zoom of the axon region, rotated and displayed to the right. Wider views are available in SI. Scale bar, 50 μ m. B) The unnormalized and normalized axon-to-dendrite expression ratio (uADR (a) and ADR (b)). Data is presented as mean \pm SEM. N=6 for each group. Kruskal-Wallis ANOVA test, ChR2-XXL versus TR5-ChR2XXL, *p=0.012<0.05, ChR2-XXL versus TR10-ChR2XXL, *p=0.009<0.01.

and B in the first image of Figure 4A. The results showed that ChR2-XXL localized to both the apical and basolateral sides of the MDCK cells (Figure 4A), while all TR-ChR2XXL targeted only the lateral membranes (Figure 4B–D). These results were unexpected as the TR sequences have been reported as apical targeting signals in epithelial cells.^[16] We discuss possible reasons for the unexpected targeting and implications for construct design below.

2.3.2. Subcellular Localization in MCF 10A Cells

Lateral targeting was persistent in other epithelial cell types. MCF 10A cells transfected with ChR2XXL or TR5-ChR2XXL were induced to form acini with polarized cell surfaces. In these spheres,

TR5-ChR2XXL was also more laterally localized than ChR2XXL (Section S6, Supporting Information). It is therefore not specific to MDCK cells that the TR-ChR2XXL combination acts as a lateral targeting signal instead of an apical signal as had been expected.

2.3.3. Subcellular Localization in Neurons

Immunostaining of TR-ChR2XXL electroporated primary neurons showed subcellular localization. Transfected neurons were immunostained with MAP2 (dendrites) and Tau1 (axons) at DIV5-7 (5–7 days in vitro). Figure 5A shows ChR2-XXL localized to both somatodendrites and axons, while TR5-ChR2XXL and TR10-ChR2XXL are mainly targeted to soma and dendrites. However, TR15-ChR2XXL produced negative effects on neuronal

ADVANCED BIOLOGY

www.advancedsciencenews.com

www.advanced-bio.com

Table 1. Transfection efficiency (TE) of actuators in different cell types in a typical independent culture.

		ChR2XXL	TR5-ChR2XXL	TR10-ChR2XXL	TR15-ChR2XXL
HEK293 (DPT2)	Expressing cells	6	12	17	11
	Total cells	83	151	266	160
	TE (%)	7.23	7.95	6.39	6.88
MDCK (DPT5)	Expressing cells	3	5	2	1
	Total cells	113	159	112	128
	TE (%)	2.65	3.14	1.79	0.78
Neuron (DIV7)	Expressing cells	20	9	3	1
	Total cells	81	93	90	129
	TE (%)	24.69	9.68	3.33	0.78

growth, such that they could not extend axons and dendrites properly. Non-transfected neurons in the same culture had normal branched dendrites and well-extended axons. Images of larger areas are provided in supplementary material (Figure S3, Supporting Information).

To quantify the degree of polarized TR-ChR2XXL distribution in cortical neurons, two forms of axon-to-dendrite expression ratio, normalized (ADR) and unnormalized (uADR), were calculated (see Experimental Section). It is advantageous to evaluate the localization of a protein according to the ADR value, as ADR = 1 means the protein is nonspecifically localized, ADR < 1 is localized to dendrites and ADR > 1 is localized to the axon. The value of uADR for ChR2-XXL (0.67 \pm 0.06) was \approx 3 times larger than that of TR5-ChR2XXL (0.20 \pm 0.05) and TR10-ChR2XXL (0.19 \pm 0.05) (Figure 5B(a)). The uADR of ChR2-XXL was significantly different from the uADR of either TR5-ChR2XXL or TR10-ChR2XXL. The ADR of TR5-ChR2XXL and TR10-ChR2XXL were 0.30 ± 0.08 and 0.28 ± 0.07 , respectively, indicating both were localized to dendrites instead of axon in neurons (Figure 5B(b)), which were consistent with the observation in MDCK cells and publications that the basolateral signal mainly corresponds to the somatodendritic signal. However, there were no ADRs for TR15-ChR2XXL-positive neurons since these cells did not have extended neurites. These results show that neurons transfected with TR5-ChR2XXL and TR10-ChR2XXL can grow normally through DIV5-7, and the expression localized to the somatodendritic region, while neuron growth was affected by the expression of TR15-ChR2XXL, perhaps due to the longer projection from the neuron membrane surface by more TRs that blocks neuronal adhesion to the substrate, thus influencing neuronal growth.

2.4. Expression in Different Cell Types

In order to investigate the applicability of the newly constructed actuators, we evaluated their expression and transfection efficiency in HEK293 cells, MDCK cells, and neurons. Transfection efficiency was not calculated for HL-1 due to the cells forming a syncytium during the time needed for expression. Transfection efficiency was not calculated for MCF 10A cells due to continual necessary modifications of the transfection protocol to achieve measurable spheroids.

2.4.1. Expression

Transfection efficiency (TE) in HEK293 cells could be extracted in parallel to electrophysiology. After chemical transfection, HEK293 cells displayed classically pyramidal or rhombic morphology, unaffected by the transgenes (Figure S4A, Supporting Information). The TEs of TR5-ChR2XXL, TR10-ChR2XXL, and TR15-ChR2XXL in HEK293 on DPT2 (2 days post-transfection) in a typical culture were 7.95%, 6.39%, and 6.88%, respectively, comparable to ChR2-XXL (7.23%) (Table 1). To facilitate the comparison in different cell types, we normalized TE to that of ChR2-XXL for each cell type. In HEK293 cells the normalized TEs were all near one (1.08 \pm 0.107, 0.91 \pm 0.050 and 0.97 \pm 0.081), and not significantly different from each other. Therefore, the plasmid update was not substantially changed by TR length.

To test TE, independent of localization, in MDCK cells, cells were plated at low density on tissue culture plastic wells for easy observation. DPT5 MDCK cells are shown in Figure S4B (Supporting Information). Generally, after growing for a certain time on a solid support, MDCK cells form cell islands. TR-ChR2XXL expression did not alter the normal morphology of MDCK cells. In an independent culture, the TE of ChR2-XXL was 2.65%, while the efficiency of TR5-ChR2XXL was a little higher at 3.14%. Whereas the efficiencies of TR10-ChR2XXL and TR15-ChR2XXL were much lower than ChR2-XXL, at 1.79% and 0.78%, respectively (Table 1). The normalized TEs of TR5-ChR2XXL, TR10-ChR2XXL, and TR15-ChR2XXL were 1.12 ± $0.046, 0.62 \pm 0.102$, and 0.24 ± 0.014 , respectively. With more TRs, the TE of MDCK cells decreased. There was a significant difference between TR5-ChR2XXL and TR15-ChR2XXL but not TR5-Cer of TRs does. Therefore, 5TR-ChR2XXL has enhanced TE in MDCK cells, while 10TR and 15TR have fewer exhR2XXL and ChR2-XXL, indicating that targeting itself in MDCK cells does not reduce TE, but the number of TRs does. Therefore, 5TR-ChR2XXL has enhanced TE in MDCK cells, while 10TR and 15TR have fewer expressing cells, though only significantly for TR15 (Figure 6). All constructs showed groups of expressing cells, indicating that transfected cells continue to divide. The decreased number of expressing cells with increasing TR in MDCK may be due to additional metabolic load slowing reproduction of larger TR expressing cells or poorer adhesion leading to loss of larger TR expressing cells.

ADVANCED BIOLOGY

www.advancedsciencenews.com www.advanced-bio.com

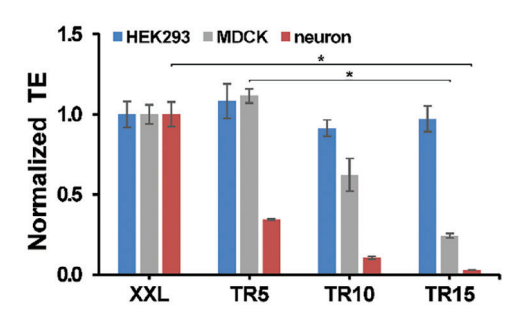


Figure 6. Normalized TEs in HEK293, MDCK, and neurons. In each cell type, the TE was normalized to ChR2-XXL. Data are mean \pm SEM, N=3 transfections for each group. Kruskal-Wallis ANOVA test, MDCK cells, TR5-ChR2XXL versus TR15-ChR2XXL, *p=0.028<0.05; neurons, ChR2-XXL versus TR15-ChR2XXL, *p=0.013<0.05.

As we cultured neurons transfected with the constructed optogenetic actuators in vitro, some unexpected changes were observed as they matured, as shown in Figure S5 (Supporting Information). Neurons transfected with ChR2-XXL were unaffected by the transgene. TR5 and TR10-tagged constructs were also expressed normally in neurons in the beginning. However, at later stages neuronal morphology degenerates. In rare cases of TR15-ChRXXL in neurons, morphology was abnormal even at the early stages of development (see Supporting Information part 5 and Discussion 3.2). TEs in neurons were evaluated on DIV7. In one typical transfection, the TEs of TR5-ChR2XXL and TR10-ChR2XXL were 9.68% and 3.33%, respectively (Table 1). However, in the TR15-ChR2XXL group, neurons could hardly express this protein, and the efficiency was only 0.78%, much lower than that of ChR2-XXL group (24.69%). The normalized TEs of TR5-ChR2XXL, TR10-ChR2XXL, and TR15-ChR2XXL were 0.34 \pm 0.005, 0.11 \pm 0.011, and 0.03 \pm 0.001, respectively. With more TRs, TE of neurons decreased, following the trend of MDCK cells. Therefore, the presence of the mucin repeats reduced the number of expressing neurons, with more TRs in the N-terminus of ChR2-XXL, the effects were more obvious with longer TRs (see also 2.4.2). Comparatively, TR effects were more obvious in polarized than in unpolarized cell types.

2.4.2. Comparison of TE

To test broader applicability, TEs in two more cell cultures were assessed. Table 1 shows the typical TEs in HEK293 cells, MDCK cells, and neurons. The results are summarized in Figure 6. TE was normalized to that of ChR2-XXL for each cell type. In neurons, the normalized TEs of TR5-ChR2XXL, TR10-ChR2XXL, and TR15-ChR2XXL were 0.34 \pm 0.005, 0.11 \pm 0.011 and 0.03 \pm 0.001, respectively. With more TRs, TE of neurons decreased. There was a significant difference between ChR2-XXL and TR15-ChR2XXL. In MDCK cells, the trend was similar, with 1.12 \pm 0.046, 0.62 ± 0.102 , and 0.24 ± 0.014 , which were higher than in neurons, particularly with TR5-ChR2XXL's TE > 1. There was a significant difference between TR5-ChR2XXL and TR15-ChR2XXL, indicating that targeting itself in MDCK cells does not reduce TE, but the number of TRs does. However, TEs in HEK293 cells were all near one (1.08 \pm 0.107, 0.91 \pm 0.050, and 0.97 ± 0.081), and not significantly different from each other. TR effects were less obvious in unpolarized than in the two polarized cell types, where more TR had lower TE. Though both polarized cell types showed a decreasing trend with number of TRs, the absolute TE in MDCK cells remained higher. For future implementation, it must be considered how to achieve high expression rates relative to the cell-specific TE, for example by enriching initially transfected cells in dividing cell cultures or exploring different plasmid transfection methods. In MDCK cells TR5-ChR2XXL and TR10-ChR2XXL were both expressed in clusters in differentiated epithelial sheets (Figure 4B,C), suggesting that lower initial TE may be overcome by allowing transfected cells to continue to divide and selecting against untransfected cells, to generate a stable cell line. Transfection in additional cell types is further discussed in the Supporting Information part 6.

3. Discussion

In the present study, three new optogenetic actuators were produced by adding different numbers of tandem repeats (TR5, TR10, and TR15) from mucin to the N-terminal of ChR2-XXL. Despite the large and likely glycosylated TRs, the optical activation still generated high currents with kinetics similar to un-tagged ChR2-XXL. In general, the construct expression in HEK293 cells was better than in polarized cells but was also not subcellularly localized. Currents could be optically triggered in both HEK293 and polarized MDCK cells. In MDCK cells, all three actuators were localized to the lateral membrane, while in neurons those that expressed (TR5-ChR2XXL and TR10-ChR2XXL) were localized to the soma and dendrites. Expression differences were observed between cell types and within a cell type according to TR length, as well as depending on culture maturity. Though we can attribute the reduced number of expressing cells with increasing TR to protein effects rather than plasmid effects, the mechanism of fewer cells remains to be determined. It may include a lower division rate of TR-expressing cells in cell lines when the construct is targeted, poorer adhesion to the substrate due to construct density, or differences in transcription rate within the cell.

Overall, among these three actuators, TR5-ChR2XXL has the best performance in cells, which could be used in particular research questions where optogenetics have as yet not been suitable. Modification of the membrane potential is critical not only in excitable cells like neurons but also in non-excitable cells like epithelia since membrane potential is the driving force for ion movement across the cell membrane, which is involved in various biological processes.^[34–36] Controlling membrane potential, calcium levels, or optogenetic tools like CRY2/CIBN or iLID/Sspb[37-40] via subcellularly targeted optogenetic constructs could have various benefits. Aside from providing spatial specificity in epithelia currents in primary cells or in vivo (see also 3.1.3) these tools could be used to improve the differentiation of epithelial organoids to better mimic organ function ex vivo. If the TR targeting motifs are fused to these proteins, more precise subcellular manipulation in complex tissues could be achieved, which would expand the applications of optogenetics in biological research. Fusion of the TR domain onto the extracellular side of other types of constructs than the directly light-gated channels may further adjust the linker domain between TRs and the main protein to avoid steric hindrance.



ADVANCED BIOLOGY

www.advanced-bio.com

3.1. Electrophysiological Characterization of TR-ChR2XXL

3.1.1. The Depolarization Properties of TR-ChR2XXL

The TR-ChR2XXLs created here behave electrophysiologically similar to ChR2-XXL (Figures 1 and 2). All have slow $au_{
m off}$ and extended open state lifetime (Figure 2G,J; Figures S1 and S2, Supporting Information), resulting in high light-evoked currents. During rapid illumination, photocurrents induce a long-lasting depolarization block (Figures 1D-I and 2A-F) due to insufficient repolarization during the slow ChR2-XXL closing. During repetitive stimulation, the photocurrents decay a little from one stimulation to the next. Comparatively, photocurrents at long pulse time and short recovery time decay more than those at shorter pulse time and longer recovery time (Figures 1F and 2E). These are all hallmarks of ChR2-XXL itself. ChR2-XXL was selected for testing TR tagging in case targeting reduced current per area achieved, for example, if targeting was due to specific degradation. Taken together, the TR tagging does not influence their continuous depolarization effect. With these high long currents, TR-ChR2XXLs are suitable for subcellularly precise optogenetic manipulation avoiding off-target effects, especially when light delivery is limiting or long-lasting depolarization is needed. This also suggests that the N-terminal of channelrhodopsins can be utilized to tag other channels with faster dynamics, which opens the way to novel expansion of the optogenetic toolbox.

3.1.2. ChR2-XXL Currents

We selected ChR2-XXL for its high currents in case targeting reduced total channel incorporation. Furthermore, since the creation of ChR2-XXL, [24] it has been applied in behavioral investigations, mainly in Drosophila, such as circadian clock, [41] locomotor behavior, [26] and spatial learning. [42] Recently, its applications even have extended from animal to plant research fields.[43,44] But unlike comparable variants such as ChR2C128A, ChR2C128S, and ChR2D156A that are well characterized, [20,45-47] few studies are about the specific electrophysiological behavior of ChR2-XXL (D156C) in response to different stimulation protocols. In addition to the targeted ChR2-XXL producing sufficient current, we have shown that the ChR2-XXL dynamics with and without TRs allow illumination sequences that increase or decrease currents based on when in the closing process channels are re-activated. Thereby our investigations help to fill in this gap and provide an important base for studying the intricate photocycle of channelrhodopsin.

In this work, all channelrhodopsins show an additional small transient current peak upon light-off in voltage-clamp mode (Figures 1 and 2), which means a larger number of open channels are accumulated transiently. This has been observed in other optogenetic channels and is attributable to the passage through the photocycle rather than the presence or absence of the tag. [28,45,47] The complex details of the channelrhodopsin photocycle intermediates (P470 $\stackrel{\circ}{\rightarrow}$ P500 $\stackrel{\circ}{\rightarrow}$ P390 $\stackrel{\circ}{\rightarrow}$ P520 $\stackrel{\circ}{\rightarrow}$ P480 $\stackrel{\circ}{\rightarrow}$ P470) are still under debate. There are two possible explanations for the current transient. The first is that the photoactivation of intermediate P480 increases current. [45,48,49] P480 is photoactive, and it forms late in the photocycle (transition 4, above), prob-

ably during channel closure.^[50] Thus, at light-off channels in prior states progress to P480 and then the transition to P470 is governed by slow kinetics. An alternative explanation considers the equilibrium modulator. Accumulation of intermediate P520 generates currents at light-on. P520 is in equilibrium with earlier nonconducting intermediate P390 (transition 3, above). When light is off, the intermediate P520 is unable to convert into nonconducting P470 instantaneously, but there are still previously formed P390 states that continue undergoing transition 3 to state P520.^[20] This transient current has been previously reported in DC gate mutants ChR2D156C, ChR2C128S,[20] and in ChR2D156A. [45,47] Overall, our work and these works together confirm that the DC gate is an important structural determinant of the channel's closing. The persistence of this unusual feature is further evidence that the TRs do not alter channel dynamics.

3.1.3. Currents in MDCK Cells

Currents produced by TR-ChR2XXL in polarized MDCK cells were generally larger per μm^2 than that in HEK293 cells (Figure 3), which likely involves the membrane geometry, native background ion currents, and TR-ChR2XXL channel distribution. Nevertheless, the trend of normalized currents in each cell type was largely due to the effect of different TRs. Unlike the slightly decreased currents in the TR-tagged group compared to the untagged group in HEK293 cells, the currents in MDCK cells were larger, reflecting more TR-ChR2XXLs in the illuminated area in MDCK cells. The more collective location in the lateral membrane meant that higher local optogenetic currents could be achieved in epithelial cells.

The plasma membrane potential of nonexcitable cells participates in diverse cellular processes to establish and maintain the morphological and functional features of epithelial cells, such as the regulation of cytoskeletal organization, [51,52] cell volume, [53,54] and wound healing. [55,56] The most common depolarization approaches used in epithelial cells are chemical, such as the addition of drugs (gramicidin, valinomycin, forskolin, etc.),[52,57,58] blockers of ion channels (phenamil, barium, amiloride, etc.)[34,58,59] and modifications of the extracellular saline composition. [52,59] However, these methods change the potentials of both the apical and basolateral membrane without spatial specificity. They also work slowly (gramicidin can only achieve its maximum depolarization 30 min after addition).^[52] The utilization of TR-ChR2XXL can improve the spatial specificity of depolarization and drastically reduce the time required for depolarization. This will help to explore the more functional roles played by basolateral membrane depolarization in biological processes, such as cytoskeletal organization signaling cascades.[51,60]

3.2. Expression in Different Cell Types

3.2.1. Expression of TR-ChR2XXL in Different Cell Types

We tested TR-ChR2XXL in the non-polarized cells HEK293 and HL-1, and the polarized cells MDCK II, MCF 10A, and primary neurons. HEK293, MDCK II, and primary neurons are presented

ADVANCED BIOLOGY

www.advanced-bio.com

here, see Supporting Information for HL-1 (Figure S6, Supporting Information) and MCF 10A (Figure \$7, Supporting Information). The expression of a specific TR-ChR2XXL varies in different cell types. Since glycosylation of TR is highly variable this likely plays the largest role. First, the specific sugar chains and the number added depend on the cell type's glycosyltransferase profile.[15,61,62] This may contribute to why TR15-ChR2XXL expressed much better in HEK293 cells than in neurons and MDCK cells (Figure 6). Second, the cell type dependence of TE may also result from the distinct stress caused by expressing exogenous proteins in different cells. In our experience, neurons are more susceptible to the metabolic stress of expressing a transgene than other cell types. Third, the glycosylation is developmentally regulated.^[15] Glycosylation level, varying from 50% to 100% of available sites, changes over time as the neuron matures. This may explain why TR5-ChR2XXL and TR10-ChR2XXL transfected neurons grow normally with well-extended dendrites and axons at the early stages but gradually display abnormal morphologies like shrunken soma, degraded neurites, and ultimately death at later stages (Figure S5, Supporting Information).

The yield of cells expressing a TR-ChR2XXL construct in a specific cell type depends on the length of TR at the protein level, rather than the DNA construct. A delicate balance is reported between adhesion and anti-adhesion forces in mucin-expressing cells.[63-65] Mucins participate in integrin-mediated cell adhesion to the extracellular matrix (ECM), mainly being dominated by their TR region. Integrin is ≈20 nm long and the extracellular domain of most membrane molecules is within 30 nm of the plasma membrane. [66,67] However, TR5, TR10, and TR15 project respectively 25, 50, and 75 nm from cell surfaces, assuming a wormlike chain with 2.5Å per amino acid. [68] The function mainly depends on the length of the TR domain. Initially, more TRs weaken the cell adhesion to ECM, but much longer TRs activate integrin clustering to increase adhesion.^[69–71] In our cases. TR-ChR2XXL containing more tandem repeats is more likely to hinder the interaction of integrin with ECM, since the more TRs, the greater its difference to the length of integrins, but the tandem repeats we used are not sufficient to indirectly activate the integrin clustering. This provides an explanation for the observations that in neurons and polarized MDCK cells there are fewer expressing cells in the cases of ChR2XXL with more TRs since the ones that are not adhered well die or are washed off. It is also suggested by the more prominent response to TR length in cells grown on an ECM-containing coating. In order to solve the negative adhesion/viability issues of TRs, two strategies were tried. First, we introduced stronger adhesion via antibody-mediated pathways. Second, integrin expression was chemically enhanced to overcome the long TRs. However, unfortunately, these treatments did not improve neuronal viability. Future work is needed to more accurately dissect the interaction of integrins, TRs, and adhesion in neuronal systems, including investigating if in vivo cell adhesion is similarly affected. Therefore, pending further information, the use of TR-tagged ChRs is better suited to epithelia.

3.2.2. Subcellular Localization of TR-ChR2XXL in Polarized Cells

The subcellular localization of all TR-tagged ChR2-XXL constructs was in the lateral membrane in MDCK cells (Figure 4).

Previous reports indicate the ectodomain of MUC1 can rather confer apical localization to basolateral CD2, [72] and the addition of TR to Tac enhanced apical delivery, but not basolateral delivery. [17] Probably, ChR2-XXL interacts with the TR motif leading to the change of the TR targeting pathway. Since the basolateral and somato-dendritic localization correlation is maintained, we do not perceive this as a misattribution in MDCK cells, but rather an altered function of TRs in our constructs. This should be considered in future design plans to expand the use of optogenetics, giving specific consideration to the tag-channel-cell combination. The extracellular domain that hindered neuronal growth in vitro may also not be as detrimental to established neuronal networks as may be achieved by inducible promoters or transduction of established networks. This would require future testing of tag-channel-cell-tissue combinations.

Additional portions of the MUC1 ectodomain or a combination of TRs with apical targeting domains from other cell types may be tested in future constructs. Other publications predominantly report somatodendritic sorting signals are frequently encoded in the cytoplasmic tails of transmembrane proteins while axonal sorting signals are usually at the extracellular or transmembrane domains of proteins. [73,74] However, we show the extracellular TR domains direct ChR2-XXL to soma/dendrites (Figure 5A,B), indicating that until we understand the complex underlying mechanisms of polarized trafficking, targeting optogenetic constructs will remain largely an empirical endeavor.

4. Conclusion

In the present work, we constructed three subcellularly-localized optogenetic actuators. ChR2-XXL was shown to provide sufficient currents with small membrane area illumination and currents at different illumination protocols show promise for stimulation, long-term depolarization with low light input, and the possibility to inhibit activity by depolarization block. Since the majority of the subcellularly-localized ChR2 are modified in their Cterminus, our work on the modification of the N-terminus opens more possibilities to use N-terminal targeting motifs with channelrhodopsins. In addition, so far most of the known subcellularly plasma membrane-targeted optogenetic works have focused on utilizing the neuron-specific targeting motifs, whereas this work verifies for the first time to our knowledge that epithelial targeting motifs can also be used for compartment-specific optogenetic actuators without limiting channel performance. Different parts of the MUC targeting domain may be investigated in future constructs to improve performance in cell types that grew poorly, as neurons did, with extensive extracellular domains. The more precise optogenetic manipulation of epithelial membrane fluxes will promote our understanding of the subcellular function of the epithelium and the whole of polarized cells. The control of ionic currents across epithelium in tissues such as lungs and kidneys could also lead to new therapeutic concepts utilizing optogenetics.

5. Experimental Section

Construct Generation: ChR2-XXL (a gift from Dr. Shiqiang Gao) was a D156C variant of Channelrhodopsin-2 (ChR2) from Chlamydomonas

ADVANCED SCIENCE NEWS ADVANCED BIOLOGY

www.advancedsciencenews.com

www.advanced-bio.com

reinhardtii with enhanced expression and extended open-state lifetime. YFP was tagged to its C-terminus (ChR2XXL-YFP). Protein ChR2XXL-YFP was encoded by plasmid psc-hSyn-ChR2XXL-YFP (6593 bp) constructed in the lab previously by Dr. Lei Jin. ChR2XXL-YFP was amplified from this plasmid through PCR with AccuPrime Taq DNA Polymerase System (Thermo Fisher Scientific, Germany). For final DNA assembly, appropriate overlapping ends were designed between adjacent fragments during amplification. ChR2XXL-YFP was primed with AAGCTTGCCACCATG-GATTATGGAG and CGGCCGCCGGCAAGTAAGGATCCACTAGTCCAGTG (overlap with downstream linear vector underlined). Mucin fragments with different tandem repeats flanked by overlaps were codon-optimized according to the codon usage database and commercially synthesized into plasmids as Strings of DNA Fragments. Each TR included GSTAP-PAHGVTSAPDTRPAP. The subclone encoding 5 tandem repeats (TR5) was synthesized by Eurofins and the subclones encoding TR10 and TR15 were synthesized by Thermo Fisher Scientific. TR fragments and their overlaps were amplified by PCR with primers TAAGCTTGGTACCGAGCTC and CTCCATAATCCATGGTGGC. The vector pcDNA4/TO was linearized with BamHI (Thermo Fisher Scientific), serving as the backbone for generating new optogenetic actuators. TR sequences were added to the Nterminus of ChR2XXL-YFP, using seamless cloning with NEBuilder HiFi DNA Assembly Master Mix (New England BioLabs, Germany), producing three new plasmids TO-TR5-ChR2XXL-YFP, TO-TR10-ChR2XXL-YFP and TO-TR15-ChR2XXL-YFP. Their lengths were 7080, 7380, and 7680 bp, respectively. The results were confirmed by DNA sequencing and digestion plus DNA agarose gel electrophoresis. New plasmids were grown in NEB Stable Competent E.coli (New England Biolabs).

Cell Culture and Gene Delivery: HEK293 cells were cultured in Dulbecco's modified Eagle's medium (Sigma-Aldrich) supplemented with 10% FBS (Life Technologies) and 100 U mL⁻¹ penicillin/streptomycin (Gibco) at 37 °C and 5% CO₂. Stock cells were cultured in T25 flasks and routinely passaged three times per week by trypsinization. HEK293 were transfected using FuGENE HD Transfection Reagent one or two days after seeding. HEK293 cells were cultured on TCP well plates for TEs tests or on PLL-coated glass coverslips for patch clamp experiments.

MDCK type II cells were maintained in Minimum Essential Medium Eagle (Sigma-Aldrich) supplemented with 5% fetal bovine serum (FBS, Life Technologies) and 2 mM L-Glutamine (Life Technologies) in T25 flasks at 37 °C and 5% CO2. Stock cultures were maintained between 20% and 90% confluency, splitting roughly every three days. MDCK cells were chemically transfected with FuGENE HD Transfection Reagent (Promega, Germany) within two days after plating. In transfection level tests, MDCK cells were grown on tissue culture plastic (TCP) well plates. Cells used for immunofluorescence staining were plated at 1×10^5 cells cm $^{-2}$ on polycarbonate filters (d=13 mm, pore size 0.4 μ m, Whatman Nuclepore Track-Etched Membranes) to grow for ≈ 5 days to develop a tight monolayer. Cells for electrophysiology were grown on pieces of polycarbonate filters (pore size 0.2 μ m) coated with PLL and the medium was supplemented with penicillin/streptomycin (100 U mL $^{-1}$, Life Technologies) and 1 μ M trans-retinal.

Cortical neurons were dissected from E18 Wistar rat embryos (Janvier, France). Cortices were digested in 0.05% Trypsin EDTA for 10 min at 37 °C followed by mechanical trituration and then cultured according to Brewer et al..[75] Before plating, neurons were electroporated with $\approx 2~\mu g$ DNA per 2 $\times~10^6$ cells using the Amaxa nucleofector system (Lonza Group Ltd, Germany). Neurons were plated onto poly-L-lysine (PLL, 10 μg mL $^{-1}$, Sigma-Aldrich, Germany) and extracellular matrix (ECM, 100 μg mL $^{-1}$, Sigma-Aldrich)-coated glass coverslips at 250 cells mm $^{-2}$. Cells were maintained in Neurobasal (NB) Medium (Life Technologies, Germany) supplemented with 1% (v/v) B-27 (Gibco), 0.5 mM L-glutamine (Gibco), and 50 μg mL $^{-1}$ gentamicin (Sigma-Aldrich) at 100% humidity, 5% CO $_2$, 37 °C. Half of the medium was exchanged with fresh NB twice per week. Neurons were obtained according to permit 81-02.04.2018.A190, by the the Landesumweltamt für Natur, Umwelt und Verbraucherschutz Nordrhein-Westfalen, Recklinghausen, Germany.

Fluorescent Immunocytochemistry and Image Analysis: For immunostaining, cells were fixed with pre-warmed 4% (w/v) paraformaldehyde (Sigma-Aldrich) in PBS for 10 min at room temperature (RT). The fixed

cells were permeabilized with 0.3% TritonX-100 (Sigma-Aldrich) in blocking buffer (BB, 1% (w/v) bovine serum albumin and 2% (v/v) heatinactivated goat serum in PBS, Sigma-Aldrich) for 10 min at RT. Cells were incubated in BB at 4 °C overnight. For neurons, the following primary antibodies were used: rabbit anti-MAP2 (dendritic marker; AB5622, Sigma-Aldrich) and mouse anti-Tau1 (axonal marker; MAB3420, Sigma-Aldrich). The secondary antibodies were goat anti-rabbit Alexa Fluor 633 (A21071, Life Technologies) and goat anti-mouse Alexa Fluor 350 (A21049, Life Technologies). MDCK cells were labeled with primary antibody mouse antipodxl (3F2/D8, contributor G.K. Ojakian of SUNY Brooklyn, obtained from the DSHB, created by the NICHD of the NIH and maintained at The University of Iowa, Department of Biology, Iowa City, IA 52242). The secondary antibody was goat anti-mouse Alexa Fluor 633 (A21052, Life Technologies). Nuclei were stained with 4',6-diamidin-2-phenylindol (DAPI, Sigma-Aldrich). Samples were mounted to glass microscope slides in Dako Fluorescence Mounting Medium (Agilent Technologies, Germany) and photographed by using an AxioImager Z1 equipped with Apotome (Carl Zeiss AG, Germany).

Images were quantified using two forms of axon-to-dendrite expression ratio, normalized (ADR) and unnormalized (uADR), via Fiji software. The mean fluorescence per pixel (F) was achieved after subtracting the background. The ratio of F in axon and dendrite of the individual actuator was calculated as the uADR. The normalized ADR was the individual uADR divided by the uADR value of the nonspecifically localized ChR2-XXL.

Electrophysiology: Electrophysiology was investigated by whole-cell patch clamp. The patch clamp setup consisted of a grounded Faraday cage, microscope, amplifier (EPC9, HEKA Elektronik Dr. Schulze GmbH, Germany), micromanipulators, pipette-holders, and computer for controlling stimulation and data acquisition (TIDA 5.240 software HEKA Elektronik Dr. Schulze GmbH).

Recordings of HEK293 cells were conducted in extracellular buffer containing in mM: 140 NaCl, 5 KCl, 5 MgCl $_2$, 10 HEPES, 1 CaCl $_2$ (pH 7.3, 248 mosm kg $^{-1}$). Patch pipettes were pulled from fire-polished borosilicate glass capillaries (O.D. = 1.5 mm, I.D. = 0.86 mm; Sutter Instrument, USA) in a micropipette puller (P-2000, Sutter Instrument), for a pipette resistance of 3–6 MOhm after filling with intracellular patch solution containing in mM: 2 NaCl, 120 KCl, 4 MgCl $_2$, 5 HEPES, 0.2 EGTA, 0.2 Mg-ATP (pH 7.3, 255 mosm kg $^{-1}$). An Ag/AgCl recording electrode and a reference electrode were used in all recordings. Experiments were performed at RT in HEK293 cells between DPT2 and DPT5 with a holding potential or holding current as indicated in the captions.

Recordings of MDCK cells used different buffers due to the cells' naturally high chloride currents and different osmolarity of the culture. The extracellular bath contained (in mM): 121 NaCl, 5.4 KCl, 1.8 CaCl $_2$, 0.8 MgSO $_4$, 6 NaHCO $_3$, 1 NaH $_2$ PO $_4$, 5.5 glucose, and 25 HEPES. The pipette was filled with (in mM): 67.5 K_2 SO $_4$, 2 NaCl, 4 MgCl $_2$, 5 HEPES, 0.2 MgATP osmolarity adjusted with glucose to 293 mosm kg $^{-1}$. Both buffers were adjusted to pH 7.3. Glucose was added to the extracellular buffer directly before measurement to match the osmolarity of the growth medium directly before the sample was transferred. Since ChR2 most strongly conducted monovalent cations, and had some calcium conduction, the expected change in driving potential for Na $^+$ and K $^+$ in MDCK versus in HEK293 buffers was <2% in both cases. Recordings were performed between DPT3 and DPT9 at a holding potential of -60 mV.

Optogenetic Manipulation: Photostimulation via a 473 nm diode laser (Rapp OptoElectronic GmbH, Germany) was controlled by UGA40 (Rapp OptoElectronic GmbH). Laser flashes were triggered by the UGA software with specific control of the pulse time, delay time and spot position. An external TTL trigger between the HEKA EPC9 and UGA40 synchronized the laser to the patch clamp. The laser light was guided into a Zeiss Axio Scope upright microscope equipped with an Olympus objective (20xW). An HXP light source (Carl Zeiss AG) with filters excitation 472/35, emission 534/30, and beam splitter 497–505 was used to identify channelrhodopsin-positive cells. The AxioCam MRm (Carl Zeiss AG) was used for image acquisition. FWHM spot size for stimulation of HEK293 cells was 113 µm² and for MDCK cells 13 µm².

Statistical Analyses: Data were analyzed in Excel, Origin, or Matlab software. All statistical significance analyses were performed using SPSS

www.advanced-bio.com

27010198, 2024, 3, Downloaded

from https://onlinelibrary.wiley.com/doi/10.1002/adbi.202300428 by Forschungszentrum

software. Shapiro-Wilk test for normality and Levene's test for homogeneity of variance were used. If these preconditions were met, a one-way ANOVA or two-way repeated ANOVA test was performed for comparison between the three groups. Otherwise, the Mann–Whitney test was applied for comparison between two groups, and Kruskal–Wallis test was conducted for comparison between three groups. The significance level was set as 0.05.

Ethics Statement: Animal usage was approved by the state animal ethics committee, Landesamt für Natur, Umwelt und Verbraucherschutz Nordrhein-Westfalen, Recklinghausen, Germany under permit number 81-02.04.2018.A190.

Supporting Information

Supporting Information is available from the Wiley Online Library or from the author.

Acknowledgements

The authors thank Bettina Breuer for cortical isolation. J.W. gratefully acknowledges financial support from the China Scholarship Council (CSC). The research was supported by the Helmholtz Association

Open access funding enabled and organized by Projekt DEAL.

Conflict of Interest

The authors declare no conflict of interest.

Author Contributions

J.W., E.N., and V.M. designed research; J.W., E.P.B, and V.M. performed research and analyzed data; J.W. wrote the paper and V.M. revised the paper; V.M. and A.O. provided critical discussion and insights; and A.O. supervised research.

Data Availability Statement

The data that support the findings of this study are available in the supplementary material of this article.

Keywords

channelrhodopsin-2, optogenetics, subcellular targeting, tandem repeats

Received: August 15, 2023 Revised: October 31, 2023 Published online: November 27, 2023

- K. Deisseroth, G. Feng, A. K. Majewska, G. Miesenböck, A. Ting, M. J. Schnitzer, J. Neurosci. 2006, 26, 10380.
- [2] Z. M. Lasiecka, C. C. Yap, M. Vakulenko, B. Winckler, Int Rev Cell Mol Biol 2009, 272, 303.
- [3] M. Bentley, G. Banker, Nat. Rev. Neurosci. 2016, 17, 611.
- [4] T. L. Lewis, T. Mao, K. Svoboda, D. B. Arnold, Nat. Neurosci. 2009, 12, 568.
- [5] T. L. Lewis, T. Mao, D. B. Arnold, PLoS Biol. 2011, 9, e1001021.
- [6] M. S. Grubb, J. Burrone, *PLoS One* **2010**, *5*, e13761.

- [7] Z. Zhang, J. Feng, C. Wu, Q. Lu, Z.-H. Pan, PLoS One 2015, 10, e0142052.
- [8] C. A. Baker, Y. M. Elyada, A. Parra, M. M. Bolton, *Elife* 2016, https://doi.org/10.7554/eLife.14193.
- [9] C. C. Y. Zofia, M. Lasiecka, M. Vakulenko, B. Winckler, Compartmentalizing the Neuronal Plasma Membrane: From Axon Initial Segments to Synapses, vol. 272, Elsevier, Amsterdam 2009.
- [10] C. G. Dotti, K. Simons, Cell 1990, 62, 63.
- [11] A. Francesconi, R. M. Duvoisin, J. Neurosci. 2002, 22, 2196.
- [12] D. Wisco, E. D. Anderson, M. C. Chang, C. Norden, T. Boiko, H. Fo?Lsch, B. Winckler, J. Cell Biol. 2003, 162, 1317.
- [13] C. C. Yap, R. L. Nokes, D. Wisco, E. Anderson, H. Folsch, B. Winckler, J. Cell Sci. 2008, 121, 1514.
- [14] G. G. Farías, L. Cuitino, X. Guo, X. Ren, M. Jarnik, R. Mattera, J. S. Bonifacino, *Neuron* 2012, 75, 810.
- [15] C. L. Hattrup, S. J. Gendler, Annu. Rev. Physiol. 2008, 70, 431.
- [16] C. L. Kinlough, P. A. Poland, S. J. Gendler, P. E. Mattila, D. Mo, O. A. Weisz, R. P. Hughey, J. Biol. Chem. 2011, 286, 39072.
- [17] X. Zheng, J. E. Sadler, J. Biol. Chem. 2002, 277, 6858.
- [18] G. Nagel, T. Szellas, W. Huhn, S. Kateriya, N. Adeishvili, P. Berthold, D. Ollig, P. Hegemann, E. Bamberg, *Proc Natl Acad Sci U S A* 2003, 100, 13940.
- [19] G. Nagel, T. Szellas, S. Kateriya, N. Adeishvili, P. Hegemann, E. Bamberg, Biochem. Soc. Trans. 2005, 33, 863.
- [20] A. Berndt, O. Yizhar, L. A. Gunaydin, P. Hegemann, K. Deisseroth, Nat. Neurosci. 2009, 12, 229.
- [21] O. Yizhar, L. E. Fenno, M. Prigge, F. Schneider, T. J. Davidson, D. J. O'shea, V. S. Sohal, I. Goshen, J. Finkelstein, J. T. Paz, K. Stehfest, R. Fudim, C. Ramakrishnan, J. R. Huguenard, P. Hegemann, K. Deisseroth, *Nature* 2011, 477, 171.
- [22] F. Schneider, C. Grimm, P. Hegemann, Annu. Rev. Biophys. 2015, 44, 167.
- [23] K. Deisseroth, P. Hegemann, Science 2017, 357, eaan5544.
- [24] A. Dawydow, R. Gueta, D. Ljaschenko, S. Ullrich, M. Hermann, N. Ehmann, S. Gao, A. Fiala, T. Langenhan, G. Nagel, R. J. Kittel, *Proc Natl Acad Sci U S A* 2014, 111, 13972.
- [25] J. Higgins, C. Hermanns, C. Malloy, R. L. Cooper, Neurosci Res 2017, 125, 1.
- [26] M. Mattingly, K. Weineck, J. Costa, R. L. Cooper, PLoS One 2018, 13, e0200107.
- [27] M. Karmažínová, L. Lacinová, Physiol Res 2010, 59, S1.
- [28] P. Thomas, T. G. Smart, J. Pharmacol. Toxicol. Methods 2005, 51, 187
- [29] C. R. Gaush, W. L. Hard, T. F. Smith, Proc Soc Exp Biol Med 1966, 122, 931.
- [30] J. D. Dukes, P. Whitley, A. D. Chalmers, BMC Cell Biol 2011, 12, 43.
- [31] M. M. P. Zegers, L. E. O'Brien, W. Yu, A. Datta, K. E. Mostov, Trends Cell Biol. 2003, 13, 169.
- [32] D. Meder, A. Shevchenko, K. Simons, J. Fullekrug, J. Cell Biol. 2005, 168, 303.
- [33] G. K. Ojakian, R. Schwimmer, J. Cell Biol. 1988, 107, 2377.
- [34] S. Chifflet, J. A. Hernández, S. Grasso, Am. J. Physiol. Cell Physiol. 2005, 288, C1420.
- [35] M. Olivotto, A. Arcangeli, M. Carlà, E. Wanke, Bio Essays 1996, 18, 495.
- [36] F. Lang, M. Paulmichl, Kidney Int. 1995, 48, 1200.
- [37] D. Boocock, N. Hino, N. Ruzickova, T. Hirashima, E. Hannezo, *Nat. Phys.* 2020, 17, 267.
- [38] M. Uroz, S. Wistorf, X. Serra-Picamal, V. Conte, M. Sales-Pardo, P. Roca-Cusachs, R. Guimerà, X. Trepat, Nat. Cell Biol. 2018, 20, 646.
- [39] L. Valon, A. Marín-Llauradó, T. Wyatt, G. Charras, X. Trepat, Nat. Commun. 2017, 8, 14396.
- [40] H. Inaba, Q. Miao, T. Nakata, J. Biol. Chem. 2021, 296, 100290.
- [41] M. Selcho, C. Millán, A. Palacios-Muñoz, F. Ruf, L. Ubillo, J. Chen, G. Bergmann, C. Ito, V. Silva, C. Wegener, J. Ewer, *Nat. Commun.* 2017, 8, 15563.

www.advanced-bio.com

27010198, 2024, 3, Downloaded

- [42] N. Meda, G. Frighetto, A. Megighian, M. A. Zordan, *Behav. Brain Res.* 2020, 389, 112616.
- [43] A. Reyer, M. Häßler, S. Scherzer, S. Huang, J. T. Pedersen, K. A. S. Al-Rascheid, E. Bamberg, M. Palmgren, I. Dreyer, G. Nagel, R. Hedrich, D. Becker, *Proc Natl Acad Sci U S A* 2020, 117, 20920.
- [44] Y. Zhou, M. Ding, G. Nagel, K. R. Konrad, S. Gao, Plant Physiol. 2021, 187, 572.
- [45] C. Bamann, R. Gueta, S. Kleinlogel, G. Nagel, E. Bamberg, Biochemistry 2010, 49, 267.
- [46] R. Prakash, O. Yizhar, B. Grewe, C. Ramakrishnan, N. Wang, I. Goshen, A. M. Packer, D. S. Peterka, R. Yuste, M. J. Schnitzer, K. Deisseroth, *Nat. Methods* 2012, 9, 1171.
- [47] M. Perny, L. Muri, H. Dawson, S. Kleinlogel, *Cell Death Dis.* **2016**, 7, e2447
- [48] M. Saita, F. Pranga-Sellnau, T. Resler, R. Schlesinger, J. Heberle, V. A. Lorenz-Fonfria, J. Am. Chem. Soc. 2018, 140, 9899.
- [49] J. Becker-Baldus, C. Bamann, K. Saxena, H. Gustmann, L. J. Brown, R. C. D. Brown, C. Reiter, E. Bamberg, J. Wachtveitl, H. Schwalbe, C. Glaubitz, *Proc Natl Acad Sci U S A* 2015, 112, 9896.
- [50] J. Becker-Baldus, A. Leeder, L. J. Brown, R. C. D. Brown, C. Bamann, C. Glaubitz, Angew Chem Int Ed Engl 2021, 60, 16442.
- [51] S. Chifflet, J. A. Hernández, Int J Cell Biol 2012, 2012, 121424.
- [52] S. Chifflet, J. A. Hernandes, S. Grasso, A. Cirillo, Exp. Cell Res. 2003, 282, 1.
- [53] F. Lang, G. L. Busch, M. Ritter, H. Völkl, S. Waldegger, E. Gulbins, D. Häussinger, *Physiol. Rev.* 1998, 78, 247.
- [54] J. A. Hernández, E. Cristina, Am. J. Physiol. 1998, 275, C1067.
- [55] S. Chifflet, J. A. Hernandez, Biomed Res. Int. 2016, 2016, 5675047.
- [56] B. Reid, M. Zhao, Adv Wound Care 2014, 3, 184.
- [57] W. V. Breuer, E. Mack, A. Rothstein, Pflugers Arch 1988, 411, 450.
- [58] M. Paulmichl, G. Gstraunthaler, F. Lang, Pflugers Arch 1985, 405, 102.
- [59] M. Paulmichl, F. Friedrich, F. Lang, Pflugers Arch 1986, 407, 258.

- [60] R. Kroschewski, A. Hall, I. Mellman, Nat. Cell Biol. 1999, 1, 8.
- [61] S. J. Gendler, J Mammary Gland Biol Neoplasia 2001, 6, 339.
- [62] K. Tachibana, S. Nakamura, H. Wang, H. Iwasaki, K. Tachibana, K. Maebara, L. Cheng, J. Hirabayashi, H. Narimatsu, Glycobiology 2006, 16, 46.
- [63] J. Wesseling, S. W. Van Der Valk, H. L. Vos, A. Sonnenberg, J. Hilkens, J. Cell Biol. 1995, 129, 255.
- [64] B. Agrawal, S. J. Gendler, B. M. Longenecker, Mol Med Today 1998, 4, 397.
- [65] K. G. Kohlgraf, A. J. Gawron, M. Higashi, J. L. Meza, M. D. Burdick, S. Kitajima, D. L. Kelly, T. C. Caffrey, M. A. Hollingsworth, *Cancer Res.* 2003, 63, 5011.
- [66] R. O. Hynes, Cell 1992, 69, 11.
- [67] J. W. Becker, H. P. Erickson, S. Hoffman, B. A. Cunningham, G. M. Edelman, Proc Natl Acad Sci U S A 1989, 86, 1088.
- [68] R. Shogren, T. A. Gerken, N. Jentoft, Biochemistry 1989, 28, 5525.
- [69] M. J. Paszek, D. Boettiger, V. M. Weaver, D. A. Hammer, PLoS Comput. Biol. 2009, 5, e1000604.
- [70] M. J. Paszek, C. C. Dufort, O. Rossier, R. Bainer, J. K. Mouw, K. Godula, J. E. Hudak, J. N. Lakins, A. C. Wijekoon, L. Cassereau, M. G. Rubashkin, M. J. Magbanua, K. S. Thorn, M. W. Davidson, H. S. Rugo, J. W. Park, D. A. Hammer, G. Giannone, C. R. Bertozzi, V. M. Weaver, *Nature* 2014, 511, 319.
- [71] M. S. Syrkina, D. M. Potashnikova, M. A. Rubtsov, Biopolym. Cell 2019, 35, 288.
- [72] L. F. Pemberton, A. Rughetti, J. Taylor-Papadimitriou, S. J. Gendler, J. Biol. Chem. 1996, 271, 2332.
- [73] A. E. West, R. L. Neve, K. M. Buckley, J. Neurosci. 1997, 17, 6038.
- [74] M. A. Silverman, R. Peck, G. Glover, C. He, C. Carlin, G. Banker, Mol. Cell. Neurosci. 2005, 29, 173.
- [75] G. J. Brewer, J. R. Torricelli, E. K. Evege, P. J. Price, J. Neurosci. Res. 1993, 35, 567.